

LBL-7569  
UC-20g  
TID-4500-R66

*c.2*

THE PRE-CUSP PHASE OF TORMAC IV AND V

M. C. Vella and B. Feinberg

RECEIVED  
LAWRENCE  
BERKELEY LABORATORY

MAY 9 1978

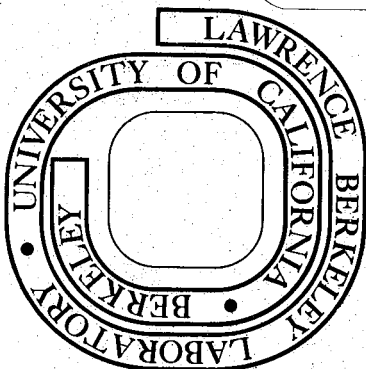
April 1978

LIBRARY AND  
DOCUMENTS SECTION

Prepared for the U. S. Department of Energy  
under Contract W-7405-ENG-48

**TWO-WEEK LOAN COPY**

*This is a Library Circulating Copy  
which may be borrowed for two weeks.  
For a personal retention copy, call  
Tech. Info. Division, Ext. ~~5716~~ 6782*



LBL-7569

*c.2*

This report was done with support from the Department of Energy. Any conclusions or opinions expressed in this report represent solely those of the author(s) and not necessarily those of The Regents of the University of California, the Lawrence Berkeley Laboratory or the Department of Energy.

THE PRE-CUSP PHASE OF TORMAC IV AND V\*

M. C. Vella

and

B. Feinberg

Lawrence Berkeley Laboratory, University of California  
Berkeley, California 94720

April 14, 1978

An heuristic analysis of the pre-cusp phase of the present Tormac experiments has been carried out. The immediate goal has been to identify the requirements for producing a stabilized pinch in Tormac V qualitatively similar to that in Tormac IV. Concurrently, V has been modified to increase the pinch current and experimental investigation is underway.<sup>1</sup> The experimental procedure<sup>2</sup> is to introduce a toroidal magnetic field into the gas filled chamber. A toroidal electric field is then induced which ionizes the gas; the associated toroidal current simultaneously pinches the discharge. Uncertainty about the details of this process, in particular, about the amount of toroidal flux trapped within the pinch, has led to a one parameter theory. Speculation about the plasma heating mechanism and the subsequent interaction of pinch and cusp is left aside at this time. The chambers are basically rectangular in cross section; but, for simplicity, an equivalent radius is used. Although the experimental discharge probably evolves into a

\*Work performed under the auspices of the United States Department of Energy.

diffuse pinch, a cylindrical sheet pinch model is studied as a first step in understanding the qualitative features of the experiment. A simple Alfven scaling for instability time scales, appropriate for the previous weak pinch and considered in the design of the ringing frequency of the induction circuit<sup>3</sup> is now supplemented by the sheet pinch model. If merited, a more quantitative numerical diffuse pinch model can be developed later. It should be pointed out that cusp confinement, the central problem of the Tormac program, is not addressed here. The goal is simply to identify the requirements for reproducing this particular phase of the Tormac IV experiment.

A comparison of some basic physical parameters of Tormac IV and V is presented in Table 1. A simple characterization of the discharge<sup>4</sup> is the initial energy of the induced current per unit chamber volume. Given a density, this can easily be reduced to the energy per particle. By this criterion, from Fig. 1, a current of 60-70 kA in V compares well with 40 kA in IV. A 25 kA case for IV is shown throughout for comparison, since it did not seem to produce the high temperatures reported for the 40 kA case. Another simple criterion is compression of the initial discharge. Consider a cylinder of radius,  $a$ , with an initial axial bias field,  $B_{z0}$ . For a low  $\beta$  plasma, the minimum surface current,  $I_{min}$ , needed for compression is set by the requirements that the poloidal pressure exceed the bias field pressure, which leads to the condition

$$I_{min} > 5a B_{z0}, \quad (1)$$

where,  $a$  is in cm,  $B_{z0}$  in Gauss, and  $I$  in Amperes. From Fig. 2, a 50 kA current with a 200 G bias field might compare with IV, but 100 kA would offer great flexibility.

After the current is induced, the plasma subsequently rearranges itself to achieve pressure balance at a new radius,  $r$ , giving,

$$B_{ZE}^2 + (I/5r)^2 = B_{ZI}^2 + 8\pi(n_e T_e + n_i T_i), \quad (2)$$

where subscripts I and E refer to the axial magnetic field inside and outside the current sheet. If  $B_{ZI}$  or, equivalently  $\beta$ , is viewed as a free parameter determined by the unspecified dynamics of the rearrangement process, this may be rewritten as,

$$B_{ZE}^2 + (I/5r)^2 = B_{ZI}^2(1 + \beta), \quad (3)$$

where

$$\beta = 8\pi(n_e T_e + n_i T_i)/B_{ZI}^2.$$

Equilibration of electrons and ions is assumed throughout. If the density and temperature used are nominal experimental values for this phase of the experiment,  $2 \times 10^{15} \text{ cm}^{-3}$  and 5 eV, respectively, the right side of (3) is determined by specifying either  $\beta$  or  $B_{ZI}$ . For convenience, it is easier to talk about  $\beta$ , but it should be remembered that this means a specific internal field, which strongly affects time scales in later considerations. The left side of (3) has two obvious unknowns  $B_{ZE}$  and  $r$ . However, energy conservation and inductive effects make  $I$  a function of  $r$ . Thus, two additional equations are needed to solve the one parameter problem. Conservation of toroidal flux requires,

$$B_{ZI}r^2 + B_{ZE}(a^2 - r^2) = B_{ZO}a^2. \quad (4)$$

This may be combined with (3) to give

$$\begin{aligned} & (B_{ZE}/B_{ZO})^3 - (B_{ZE}/B_{ZO})^2 \\ & + (B_{ZE}/B_{ZO}) \left[ (I/5a B_{ZO})^2 - (B_{ZI}/B_{ZO})^2(1 + \beta) \right] \\ & + (B_{ZI}/B_{ZO})^2(1 + \beta) - (I/5a)^2 \frac{B_{ZI}}{B_{ZO}^3} = 0. \end{aligned} \quad (5)$$

Conservation of toroidal field energy and inductive current energy may be written,

$$\begin{aligned} \frac{\pi R}{4} \left[ B_{ZI}^2 r^2 + B_{ZE}^2 (a^2 - r^2) \right] + \frac{1}{2} L(r) I^2(r) \\ = \frac{\pi R}{4} B_{ZO}^2 a^2 + \frac{1}{2} L(a) I^2(a), \end{aligned} \quad (6)$$

where the inductance is taken as

$$L(r) = 3.19 \times 10^{-8} R \left[ \ln(8R/r) - 2 \right] \text{ (H)},$$

with  $R$  the major radius and  $r$  the minor radius of the pinch. Equations (5) and (6) have been solved numerically for values of  $\beta$  from 0.5 to 0.001, or equivalently, for  $B_{ZI}$  from 1.27 to 28.4 kG. In general, three solutions are obtained from (5), one of which corresponds to expansion,  $r/a > 1$ , and is automatically rejected. A field reversed solution,  $B_{ZE}/B_{ZO} < 0$ , which requires additional energy, is also rejected. Typically, the energy conserving solution which remains corresponds to a relatively small minor radius,  $r/a < 0.2$ , with  $B_{ZE}/B_{ZO}$  approximately 0.9. However, with 100 kA,  $V$  has enough energy that a reversed field state may be energetically accessible. From Fig. 3, the entire parameter range (i.e.,  $B_{ZI}$ ) considered here is seen to be consistent with the experimental observation<sup>4</sup> that  $r \leq 2$  cm. The increased inductance of the pinched discharged is primarily responsible for reduction of the current to a final value,  $I_f$ , which, from Fig. 4, is a half to a quarter of the initial value.

Plasma pinches are often discussed in terms of either the Tokamak safety factor,  $q = aB_T/RB_P$ , or the pinch parameter,  $\theta = B_P/B_T$ , where the subscripts P and T refer to poloidal and toroidal components, and  $\theta$  is

obtained from  $B_p$  at the minor radius,  $a$ . Since Tormac IV was operated in an unstable Tokamak mode ( $q < 1$ ), the pinch parameter may be a more natural figure of merit. Z-pinch experience indicates<sup>6</sup> that the most stable discharges were obtained for  $1.2 \leq \theta \leq 2$ . For  $\theta > 2$ , very rapid, short wavelength relaxation to a stable ( $\theta \leq 2$ ) regime has been observed.<sup>7</sup> The nominal initial current and bias field values have been used to calculate  $\theta$  for the Tormac pinches. From Fig. 5, this appears to be a relevant characterization of the pre-cusp pinch. The fact that IV, with 40 kA, has  $\theta = 2.4$  indicates that short wavelength instabilities can play a role in the experiment.

The pinch current is actually induced by an oscillating L-C circuit, and the nature of instabilities which might grow in a quarter of the oscillator period may play an important role in later experimental performance. For example, long wavelength instabilities could cause the pinch to hit the wall, and are to be avoided. On the other hand, it has been suggested<sup>4</sup> that short wavelength instability could cause the pinch to kink, and subsequent interaction with the cusp fields might account for the ion heating reported in IV. In any case, instability time scales are certainly relevant, and some instability has previously been reported during 30 kA operation of V.<sup>8</sup> The simplest estimate of a time scale for long wavelength instability is the Alfvén time around the major circumference,

$$\tau_A = 2\pi R/v_A, \quad (7)$$

where  $v_A = B_{ZI}/(4\pi n_i m_i)^{1/2}$ . In Fig. 6, the number of Alfvén times in a quarter period of the preionizer circuit is shown for the parameter range of  $B_{ZI}$  considered here. This simple model indicates that long wavelength instability might be a problem only in the 28.4 kG case. Both the nominal

induced current and the oscillator period depend on circuit inductance, which is reflected in the coincidental overlap of the curves for IV and V with 100 kA. An improved estimate of growth times may be obtained by combining the results of the previous sheet pinch model with a well known MHD analysis of sheet pinch stability.<sup>9</sup> The growth rate of the dangerous m=1 mode is given by

$$\gamma = \frac{B_{ZI}}{r(4 \pi n_i)^{1/2}} \left\{ -k^2 r^2 + \left( \frac{I}{5rB_{ZI}} \right)^2 \frac{kr I_1'(kr)}{I_1(kr)} + \left[ (kr B_{ZE}/B_{ZI}) - (I/5r B_{ZI}) \right]^2 \frac{I_1'(kr) K_1(kr)}{I_1(kr) K_1'(kr)} \right\}^{1/2}, \quad (8)$$

where  $I_1$  and  $K_1$  denote Bessel functions of imaginary argument. The growth of long wavelength instabilities, which are most destructive to confinement, has been examined by taking  $kr = r/R$ . The other parameters in (8), e.g.,  $I$ ,  $r$ , and  $B_{ZI}$ , have been obtained from the results of the previous model, i.e., equations (4-6). The number of long wavelength growth times in a quarter period is shown in Fig. 7; this appears to rule out the 28.4 kG case and makes the 8.97 kG case questionable. Once again, however, V with 100 kA compares favorably with IV throughout the  $B_{ZI}$  parameter range. Equation (8) has also been used to numerically find the maximum growth rate, which tends to be at short wavelength compared to the major radius. The maximum number of growth times is shown in Fig. 8. Short wavelength growth dominates long throughout the parameter range, and only for the 1.27 kG case would short wavelengths not play a role. A strong tendency for the low  $\beta$  discharges to have short wavelength instability is suggested by this analysis.

All indications of the simple sheet pinch model considered here are that, regardless of the details of trapping the toroidal flux, with 100 kA,

the pre-cusp phase of V should reproduce this phase of the Tormac IV experiment. The most serious deficiency of present calculations for predictive purposes is the need for a single free parameter,  $B_{ZI}$ , which is not known experimentally. This is alleviated somewhat by the good comparison in terms of dimensionless parameters of the 100 kA case throughout the range of  $B_{ZI}$ . If experimental results indicate that the pre-ionizer merits further investigation, a numerical dynamical diffuse pinch model could be constructed which would also be capable of addressing the interaction of the pinch and cusp.

ACKNOWLEDGEMENTS

The authors wish to thank M. A. Levine and B. Myers for many informative discussions about Tormac IV, R. Shaw for useful criticism of an early manuscript, and R. Niland for advice on numerical work. One of the authors (M. C. Vella) especially wishes to thank H. L. Berk for his encouragement and support.

REFERENCES

1. I. G. Brown and B. Feinberg.
2. C. R. Gallagher and M. A. Levine, AFCRL-TR-74-0122; M. A. Levine and W. B. Kunkel, EPRI Proposal (1974).
3. B. Feinberg and M. A. Levine, private communication.
4. M. A. Levine, private communication.
5. B. R. Myers, private communication.
6. H. A. B. Bodin, Pulsed High Beta Plasmas, Ed. D. E. Evans, Pergamon (1975).
7. E. P. Butt, C. W. Gowers, R. F. Gribble, Yin-An Li, A. A. Newton, D. C. Robinson, J. C. Taylor, W. J. Sharp, A. J. Verhage, and H. A. B. Bodin, 6th Conference on Plasma Physics and Controlled Nuclear Fusion, CN-33/E 9.2, Tokyo (1974).
8. B. Feinberg, I. G. Brown, and M. A. Levine, Bull. APS 22, 1067 (1977).
9. B. B. Kadomstev, Reviews of Plasma Physics, Vol. 2.

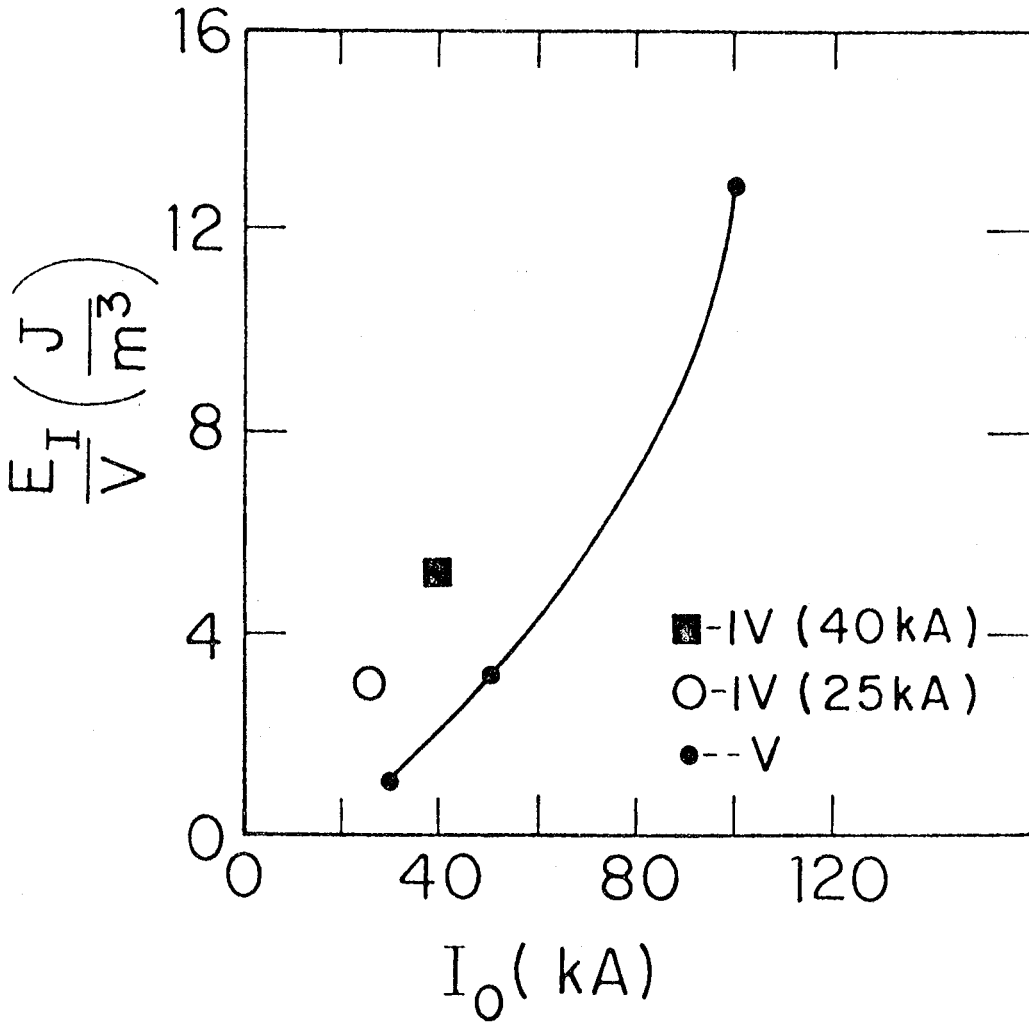
Table 1 Machine Parameters

	Major Radius R(cm)	Equivalent Minor Radius* a(cm)	Initial Current (kA)	Pre-Ionizer Frequency (k Hz)	Nominal current Energy (J)
IV	17.0	11.2	30	100	127
			40	100	225
V	34.0	18.6	30	30	270
			50	30	750
			100	50	3000

\*The equivalent radius of a circular cross section,  $a = (1 \times w/\pi)^{1/2}$ .

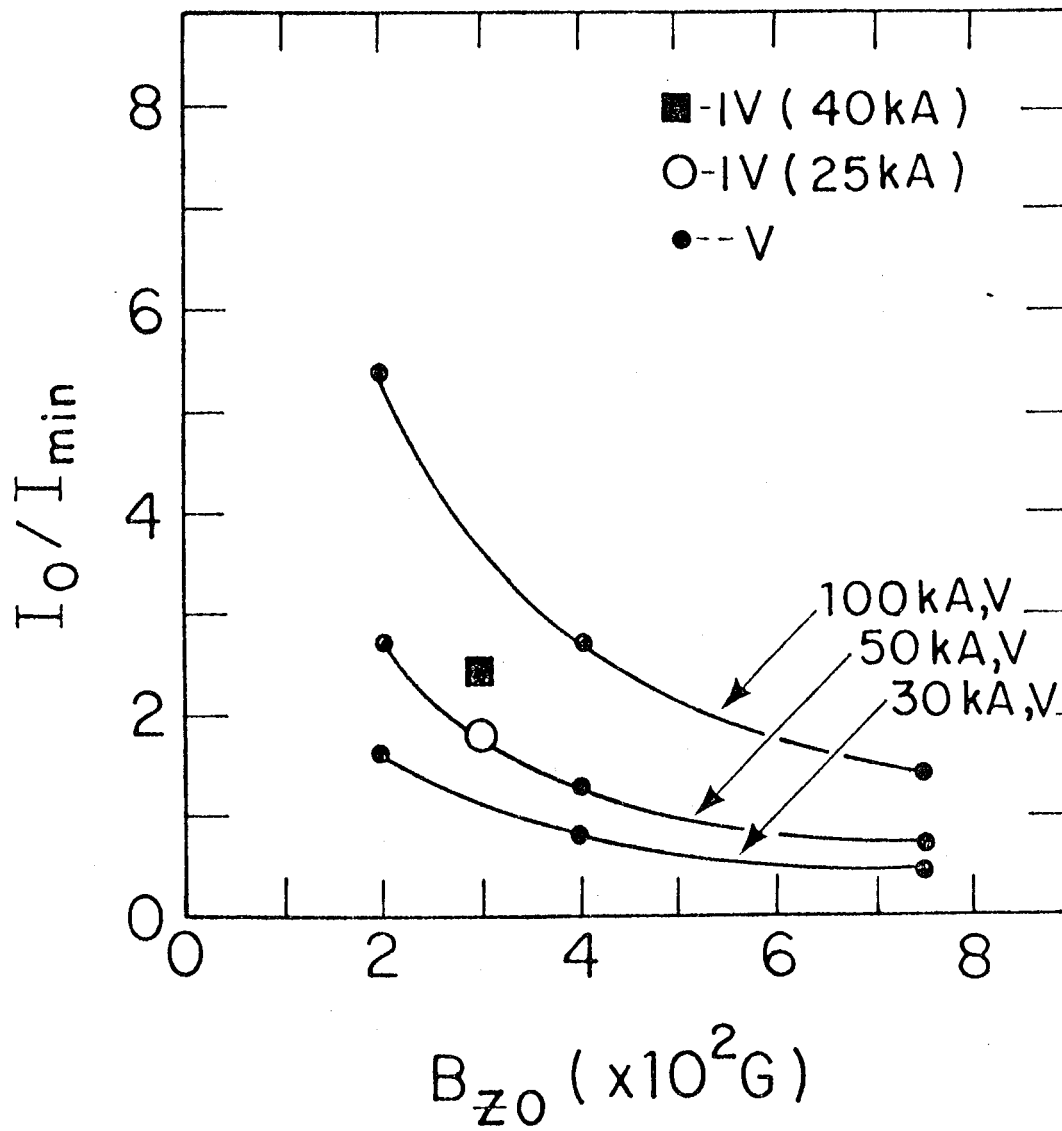
FIGURE CAPTIONS

- Fig. 1. Current energy per unit volume,  $E_T/V$ , shown as a function of normal initial current,  $I_0$ .
- Fig. 2. Comparisons of initial current,  $I_0$ , with the minimum current,  $I_{\min}$ , required to compress the initial bias field,  $B_{z0}$ .
- Fig. 3. The final pinch radius  $r$ , shown as a function of trapped fields  $B_{zI}$ ; arrows are used to indicate the range of bias field 200 to 750 Gauss.
- Fig. 4. Final pinch current  $I_f$  over the range of the free parameter,  $B_{zI}$ .
- Fig. 5. The Z pinch parameter  $\theta_{z0}$  of the initial discharge as a function of the initial bias field.
- Fig. 6. The number of Alfvén times,  $\tau_{pI}/\tau_A$ , in a major radius throughout the range of the free parameter  $B_{zI}$ .
- Fig. 7. The number of wave long wave length  $kr = r/R$ , growth times in a preionization period  $\tau_{pI}/\tau_R$ .
- Fig. 8. The maximum number of short wave length growth times in a preionization period,  $\tau_{pI}/\tau_{\max}$ .



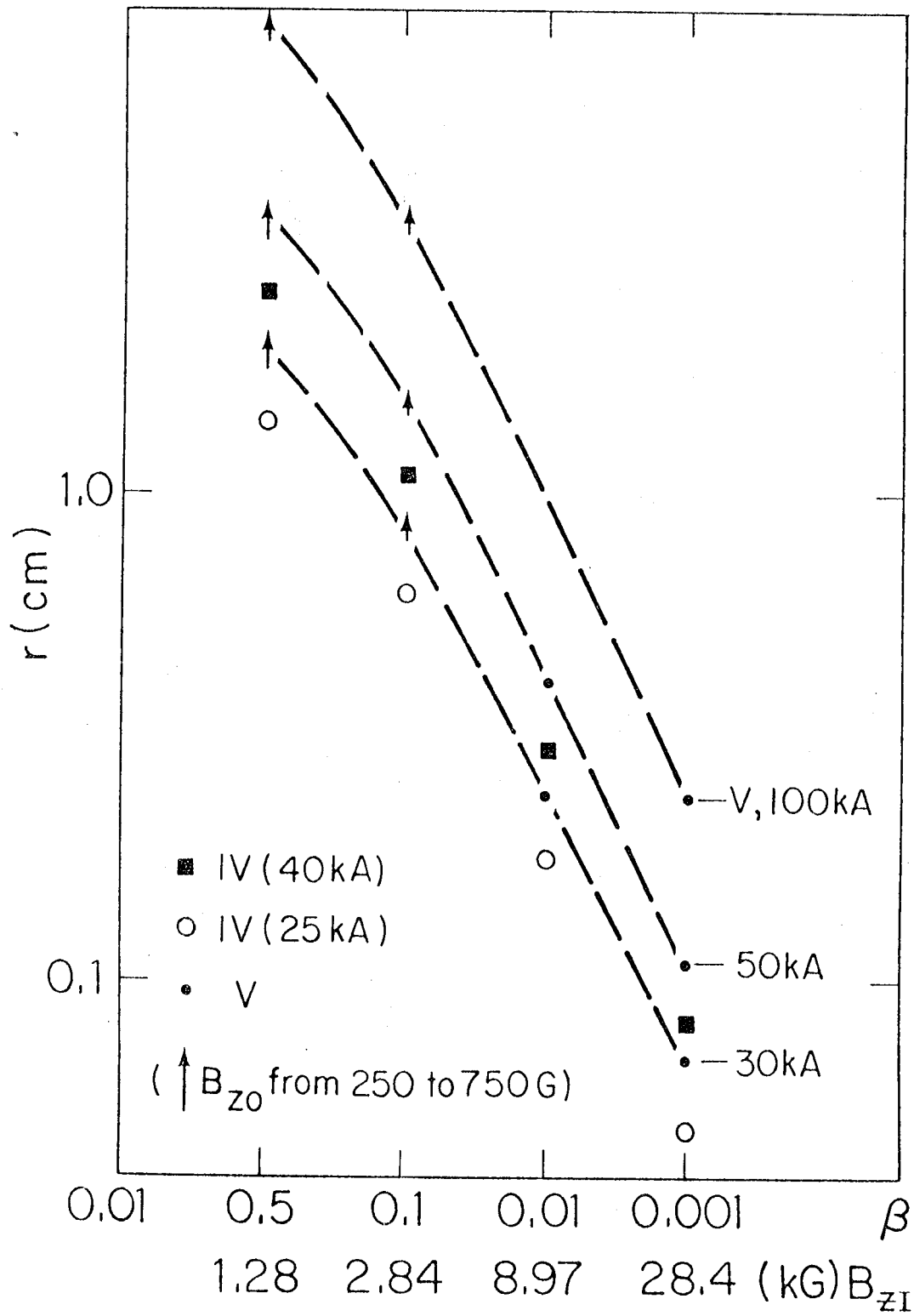
XBL 784-543

FIG. 1



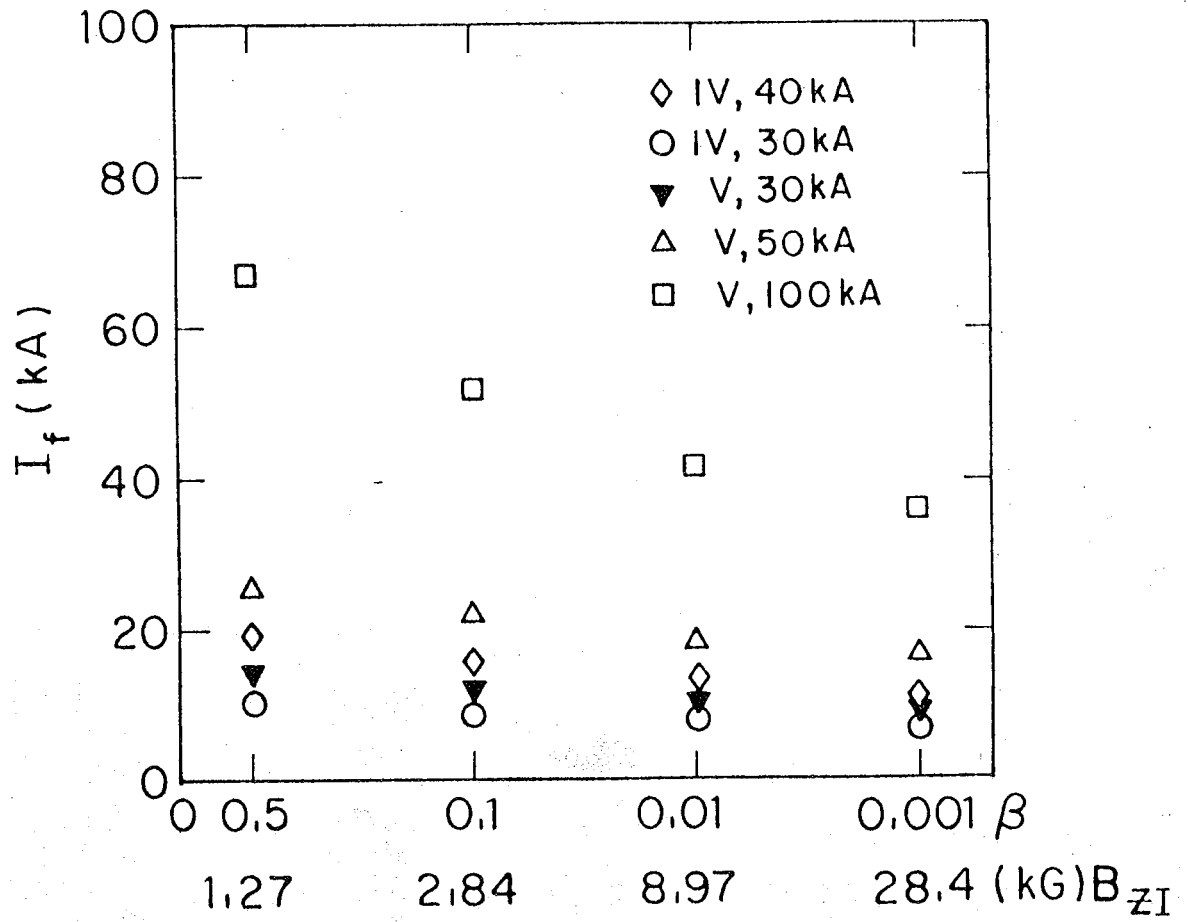
XBL 784-541

FIG. 2



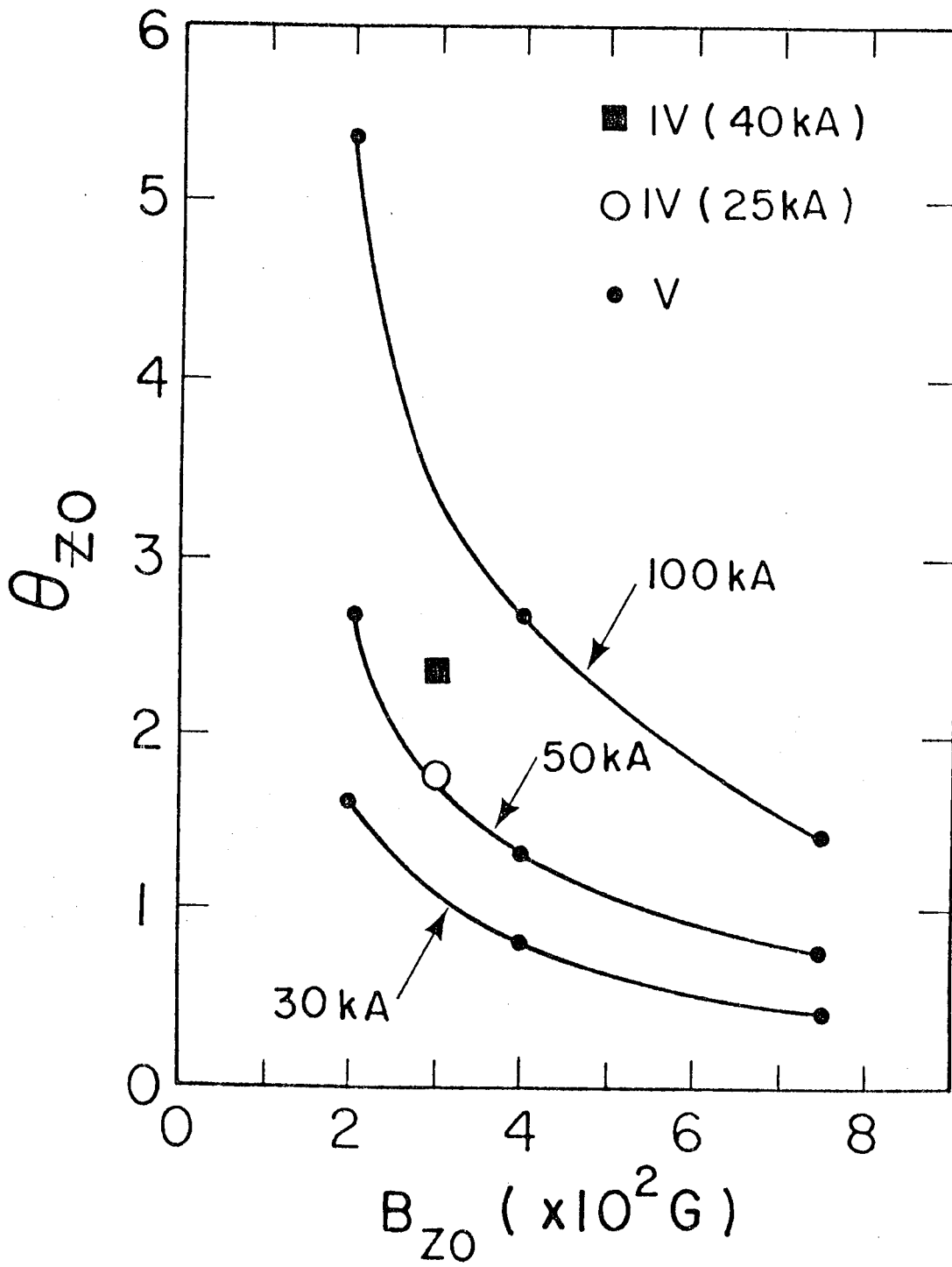
XBL 784-545

FIG. 3



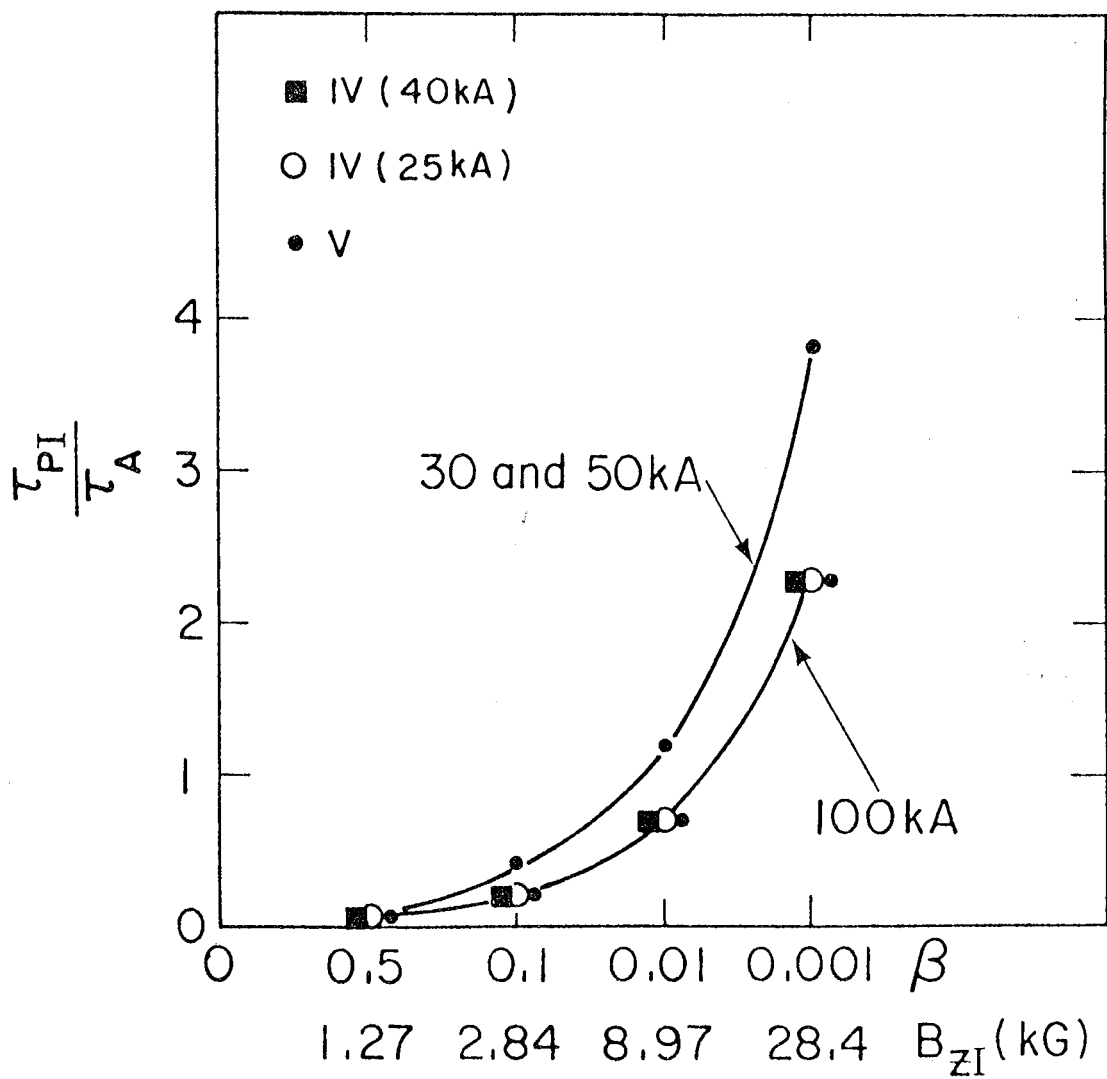
XBL 784-544

FIG. 4



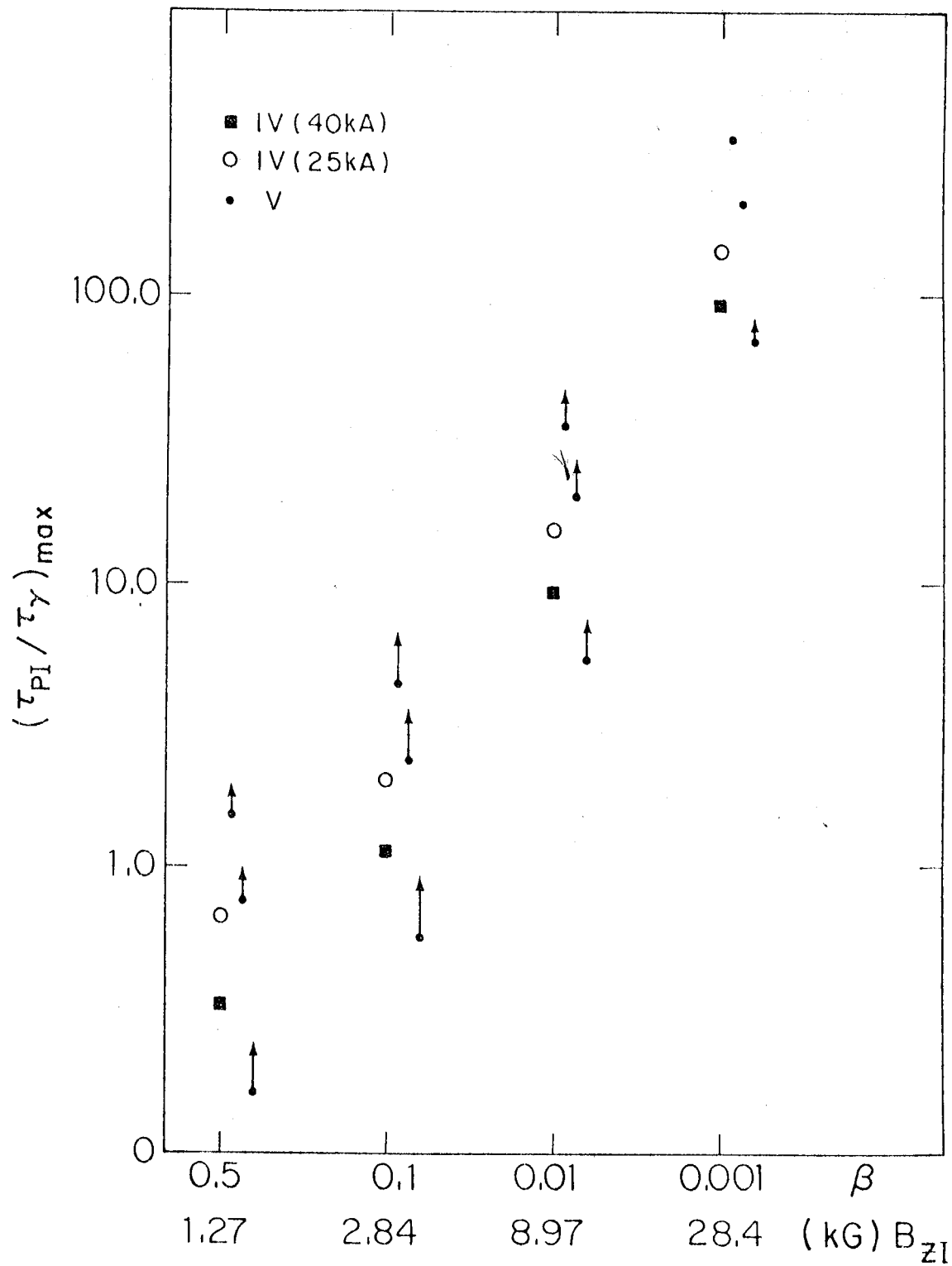
XBL 784-542

FIG. 5



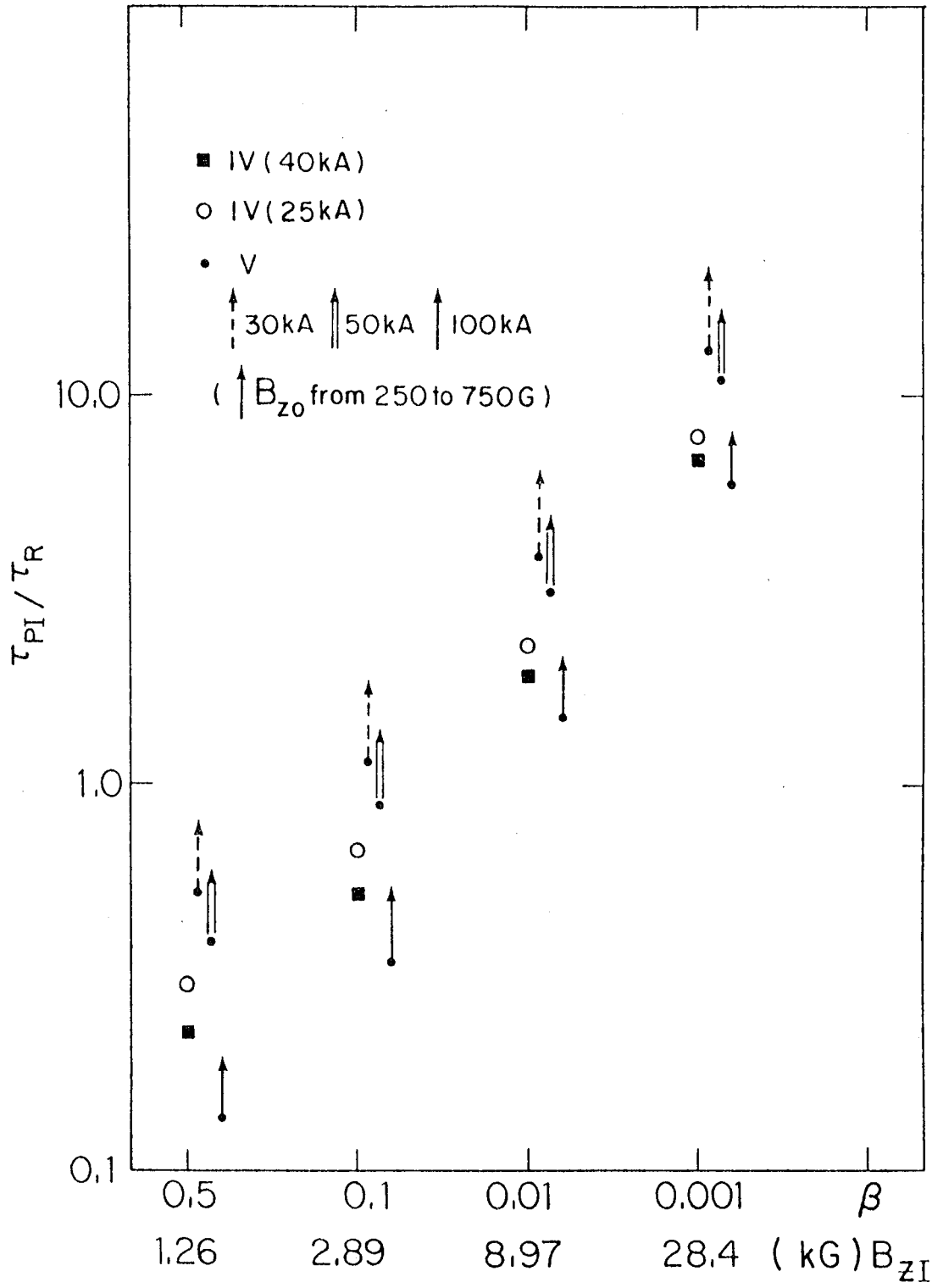
XBL 784-548

FIG. 6



XBL 784 547

FIG. 7



XBL 784-546

FIG. 8

